Structural Chemistry (2019) 30:937–944
https://doi.org/10.1007/s11224-018-1238-6

ORIGINAL RESEARCH

Theoretical investigation of the gas-phase reaction of NiO^+ with ethane

Zhao-Xuan Yuan[1] · Yong-Cheng Wang[1]

Received: 18 September 2018 / Accepted: 14 November 2018 / Published online: 5 December 2018

Abstract

To explore the mechanisms for Ni-based oxide-catalyzed oxidative dehydrogenation (ODH) reactions, we investigate the reactions of C_2H_6 with NiO^+ using density functional calculations. Two possible reaction pathways are identified, which lead to the formation of ethanol (path 1), ethylene and water (path 2). The proportion of products is discussed by Curtin-Hammett principle, and the result shows that path 2 is the main reaction channel and the water and ethylene are the main products. In order to get a deeper understanding of the titled reaction, numerous means of analysis methods including the atoms in molecules (AIM), electron localization function (ELF), natural bond orbital (NBO), and density of states (DOS) are used to study the properties of the chemical bonding evolution along the reaction pathways.

Keywords Density functional theory · Reaction mechanisms · Bonding analysis · Curtin-Hammett principle

Introduction

As the most abundant members among the saturated hydrocarbon family, alkanes are always being the most important raw materials in chemical synthesis [1–3]. However, owning to the stability of alkanes, it is difficult to selectively transform them into other compounds [4]. Therefore, chemists have been spending decades in searching for suitable catalysts to activate the inert C-H bond. A significant number of theoretical and experimental research have proved that the transition metal ions play an important role in the activation of alkanes [5–11]. Conversely, unlike propane and other higher alkanes, both methane and ethane do not activate by the late 3d transition metal ions (e.g., Fe^+, Co^+, Ni^+) at thermal energy [12, 13]. Thus, the gas-phase reactions of transition metal oxide cations with methane and ethane have attracted significant concern [14–17]. The relative experiments have been thoroughly explored by numerous mass spectrometry techniques [16, 18–22]. So far, most of the reported theoretical studies are focus on the activation of methane oxidation by late transition metal oxides that can form methanol by the direct abstraction of a hydrogen atom [23]. But few reactions of transition metal oxide cations with ethane have been reported.

In the early years, Schuurman's group used temporal analysis of product (TAP) to explore the catalytic mechanism of oxidative dehydrogenation of ethane on NiO. They found that the formation of ethylene is the main reaction channel, and the ethylene selectivity does not vary to a large extent when temperature increases [24]. Li's group also found that NiO shows a higher selectivity towards ethylene in the reaction using Weiss magnetic measurement [25]. After that, Lemonidou's group also made a predication on the reaction using isotopic labeling method, and the results indicates that the C-H bond scission is the rate-determining step in the oxidative dehydrogenation of ethane [26]. However, a detailed theoretical study for the activation of ethane by NiO has not been reported. Herein, we present a theoretical study of the gas-phase reaction of the metal oxide cation NiO^+ with ethane (298.15 K), and we find two potential chemical processes:

$$NiO^+ + C_2H_6 \rightarrow Ni^+ + C_2H_5OH \quad (1)$$

$$NiO^+ + C_2H_6 \rightarrow NiOH_2{}^+ + C_2H_4 \text{ or } NiC_2H_4{}^+ + H_2O \quad (2)$$

The reaction of NiO^+ with ethane attracts our attention for two reasons. First, as a promising catalyst, NiO^+-based materials show a significant reactivity towards alkanes [27, 28]. Thus, the theoretical study of NiO^+ with ethane can provide a guidance for comprehending the mechanism of other similar reactions. Second, the two chemical processes of titled

Electronic supplementary material The online version of this article (https://doi.org/10.1007/s11224-018-1238-6) contains supplementary material, which is available to authorized users.

✉ Yong-Cheng Wang
ycwang@163.com

[1] College of Chemistry and Chemical Engineering, Northwest Normal University, Lanzhou 730070, Gansu, People's Republic of China

reaction lead to different products. Therefore, finding out the proportion of products will provide a theoretical support for experimental research. The goal of this work is to characterize the elementary steps along the reaction pathway using DFT calculations.

Calculation methods

All calculations reported in this work were performed using the Gaussian 09 package [29]. In this paper, stationary points of doublet and quartet states in the reaction system were fully optimized using (U)B3LYP method [30]. The standardized 6-311++G(3df, 3pd) [31] basis set is used for C, H, and O atoms. The Stuttgart relativistic effective core potential (ECP) SDD is used for Ni atom. Vibrational analysis was performed to characterize all stationary points on the PESs as local minima or transition states and to evaluate the zero point energies (ZPE) included in all energies reported. Local minima on the potential energy surface (PES) have no negative eigenvalue, and saddle points have only one negative eigenvalue. The intrinsic reaction coordinate (IRC) [32, 33] was used to check if the correct transition state was properly connected to the two adjacent intermediates.

The wavefunction files (.wfn) produced by Gaussian 09 were employed as inputs into Multiwfn [34] to gain a deeper understanding of bonding analysis along the reaction pathways. So, the electron localization function (ELF) [35] used to show maxima at the most probable positions of localized electron pairs and each special position is surrounded by a basin in which there is an increasing probability to find an electron pair [36]. Besides, we also used the atoms in molecules (AIM) [37] to analyze topological properties of the (3, − 1) bond critical points (bcp) in the electron density gradient field in terms of finding out the interaction between different atoms. Similarly, the natural bond orbital (NBO) analysis was also employed in this paper in order to get a deeper understanding of the bonding information along reaction pathway. Density of states (DOS) were created, with the aim of understanding the contribution of different orbitals to the initial complex.

Results and discussion

The theoretical calculation at the (U)B3LYP/6-311++G(3df,3pd) U SDD level was performed to explain the reaction mechanisms of NiO^+ with ethane in the gas phase. All schematic structures and main parameters of all stationary and transition points on doublet state and quartet state are illustrated in Fig. 1 and Fig.S1, respectively. The possible PESs are shown in Fig. 2. The relevant energies of all species are listed in TableS2. The orbital interaction diagram of the initial complex is directly depicted in Fig. 3. In addition, bonding analysis of all species along the reaction pathways is performed, which is depicted in Fig. 6 and Table.S1. As we can see in Fig. 2, two different reaction pathways are energetically feasible, producing different products: ethanol, ethylene, and water. In the following section, detailed analysis will be gradually given.

Reaction mechanism

As the beginning of the reaction (Fig. 2a), there are two processes for C_2H_6 oxidized by NiO^+, forming two types of initial complexes: IM1a and IM1b. The two initial complexes differ based on the linkage of NiO^+ with ethane. The ^{2}IM1a(C_1) and ^{4}IM1a(C_s), which have side-on coordination pattern, are 74.8 and 113.7 kJ/mol lower in energy than the reactants; while both ^{2}IM1b and ^{4}IM1-b, which have end-on coordination pattern have C_s structures, and the relative energies to the reactants are − 43.7 kJ/mol and − 111.5 kJ/mol, respectively. It is obvious that the ^{4}IM1a and ^{4}IM1b with lower energy are more stable, which reflects the reaction starts on the quartet state.

Along the reaction pathways, through a H-shift (H3 atom to O atom), both two initial complexes can form IM2, which lies at − 268.7 kJ/mol on its doublet state and − 212.2 kJ/mol on its quartet state. The relevant transition states, TS1a and TS1b, lie at − 31.1 (− 51.9) and − 22.4 (− 26.2) kJ/mol on doublet (quartet) state. It is clearly shown in Fig. 2a that a quartet-to-doublet crossing exits after TS1a and TS1b. Therefore, starting from IM2, the reaction will proceed on the doublet state.

Once $(C_2H_5)Ni^+(OH)$ (IM2) is formed, the reaction can take place along two pathways. The first one is the formation of ethanol. With the subsequent coupling of the metal and O atom, $Ni^+(C_2H_5OH)$ (IM3-1) is formed. The bond distances of O-C1 on doublet (quartet) state is 2.068 (2.725). During this process, a barrier of 86.0 kJ/mol (26.3 kJ/mol) on its doublet (quartet) needs to be overcome. Direct dissociation of $Ni^+(C_2H_5OH)$ accounts for the generation of ethanol and Ni^+. In addition, the relative energy of $Ni^+(C_2H_5OH)$ is much lower than that of $Co^+(C_2H_5OH)$ (− 71.5 kcal/mol at B3LYP/DZVP(opt+3f):6-311+G(2d,2p)) [23] and $Fe^+(C_2H_5OH)$ (− 55.6 kcal/mol at B3LYP/DZVP(opt+3f):6-311+G(2d,2p)) [38], which indicates the more stable $Ni^+(C_2H_5OH)$ is.

Alternatively, with a stepwise β-H immigration, $(C_2H_4)Ni^+(OH_2)$ (IM4-2) could also be formed from IM2 (Fig. 2b). This formation can be divided into two steps: β-H-shift to metal center (IM2 → TS2-2 → IM3-2) and hydride H-shift to form the final complexes (IM3-2 → TS3-2 → IM4-2). During the first step, H8 atom generally moves to Ni atom to form H8-Ni bond, and the Ni-H8 distance of ^{2}IM3-2 (1.437 Å) is shorter than that of ^{4}IM3-2 (1.628 Å). This process needs to overcome a high barrier on its quartet state (115.2 kJ/mol) and a low barrier on its doublet state

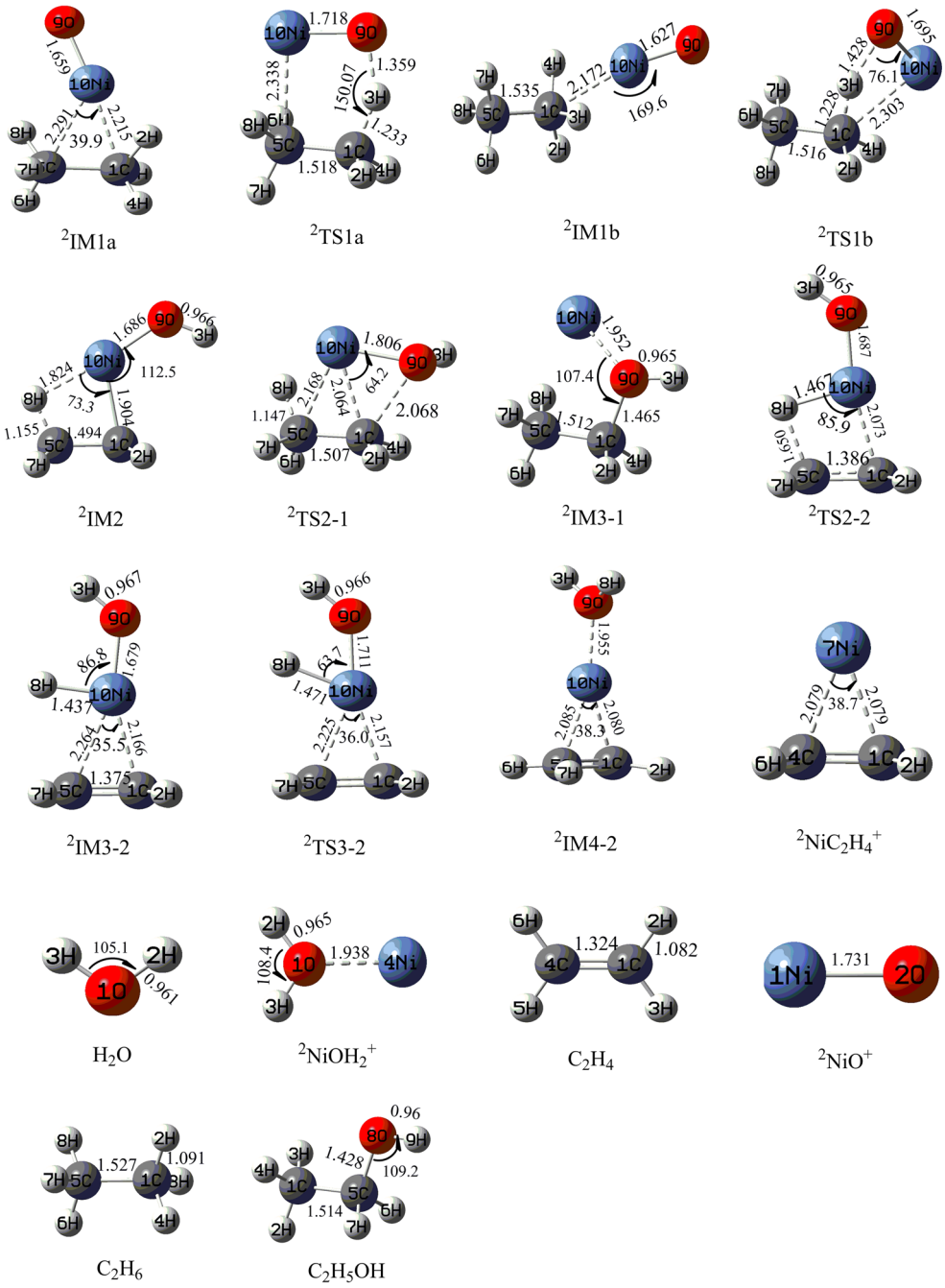

Fig. 1 Geometrical parameters of all species involved on the doublet PES at the UB3LYP/6-311++G(3df,3pd) level (bond lengths in angstrom and angles in degrees)

(57.4 kJ/mol). As to the second step, H8 atom continues to immigrate from Ni atom to O atom to form intermediate IM4-2 through the transition state TS3-2, which lies at − 215.8 (− 73.4) kJ/mol on doublet (quartet) state.

It should be noted that the final complexes (IM4-2) on both states can be described as discoordination of metal center, although ^{2}IM4-2 and ^{4}IM4-2 have a big difference in structure. In doublet, the relatively short distance between Ni^+, C_2H_4, and H_2O results in the strong stability of the ^{2}IM4-2 (ΔE_R = − 454.5 kJ/mol). Different bond cleavage of C_2H_4-Ni^+-H_2O results in different products: $Ni^+(C_2H_4)$ + H_2O or $Ni^+(H_2O)$ + C_2H_4, with the exothermicities of − 324.1 (− 314.4) and − 159.5 (− 190.9) kJ/mol on doublet (quartet) state, respectively.

Inspection of the reactions of NiO^+ with ethane, experiments found that the formation of ethylene is the main reaction channel [24, 25], which is also confirmed by our theoretical results that the ^{2}IM2 → ^{2}IM3-2 (produce ethylene and water) has the lower reaction barrier. Besides, the calculated PESs suggest that the rate-determining step of the titled reaction is the initial C-H activation located at − 31.1 kJ/mol, which is consistent with the experiment result [26].

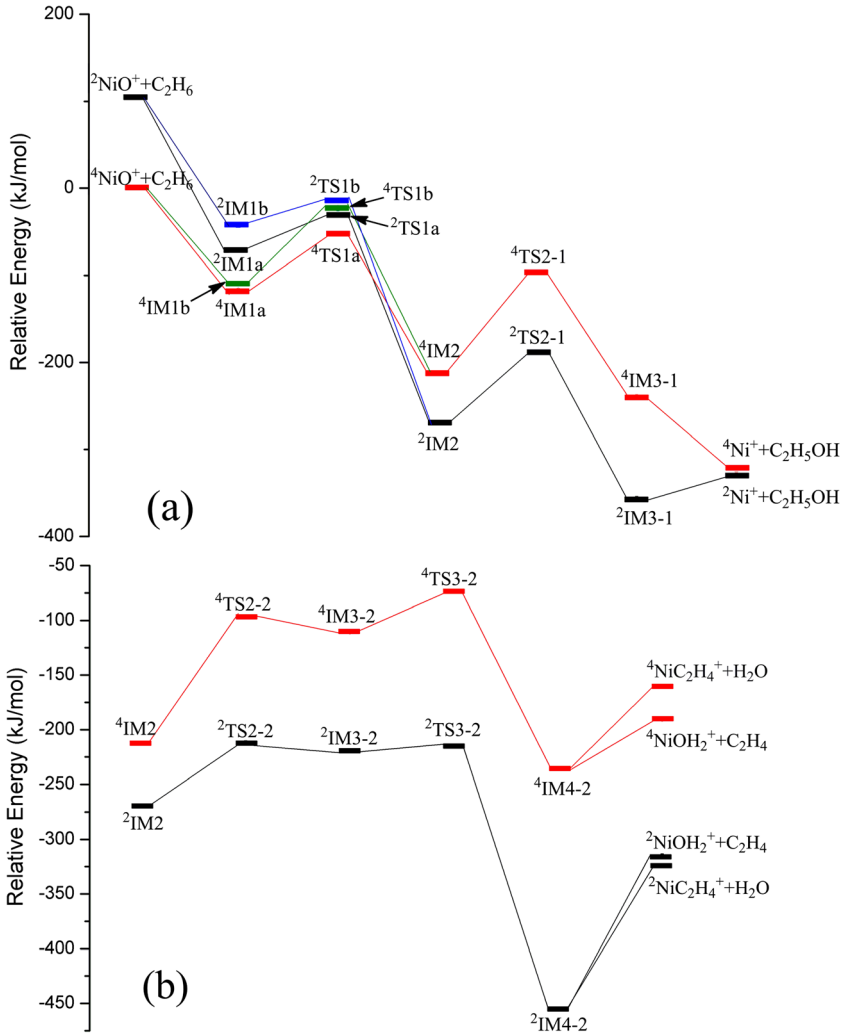

Fig. 2 Potential energy profile for the reaction of NiO^+ with C_2H_6 at the UB3LYP/6-311++G(3df,3pd) level of theory. **a** The loss of ethanol involved in the C_2H_6 oxidation by NiO^+. **b** The loss of ethylene and water from complex $(C_2H_5)Ni^+(OH)$ involved in the C_2H_6 oxidation by NiO^+

Initial complexes

The connection of NiO^+ and C_2H_6 forms two initial complexes, IM1a and IM1b. To gain a deeper understanding of how fragment orbitals are mixed to form complex orbital, the orbital interaction diagrams are plotted in Fig. 3. The DOS analysis (Fig. 4), which is composed of density of states (TDOS) and partial density of states (PDOS), is also used in this section in order to get more information about the composition of the highest occupied molecular orbital (HOMO). The vertical line shows the position of the HOMO. As shown in Fig. 3, the left and right horizontal lines represent for the

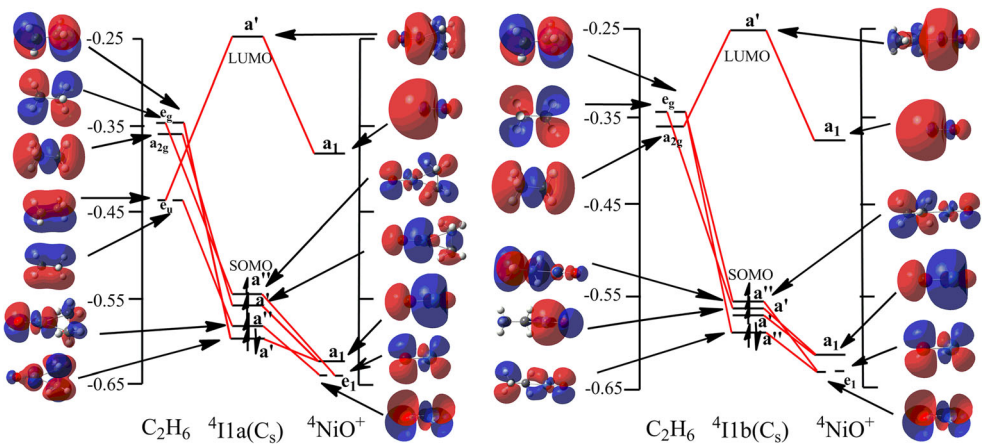

Fig. 3 Orbital interaction diagram of initial complexes

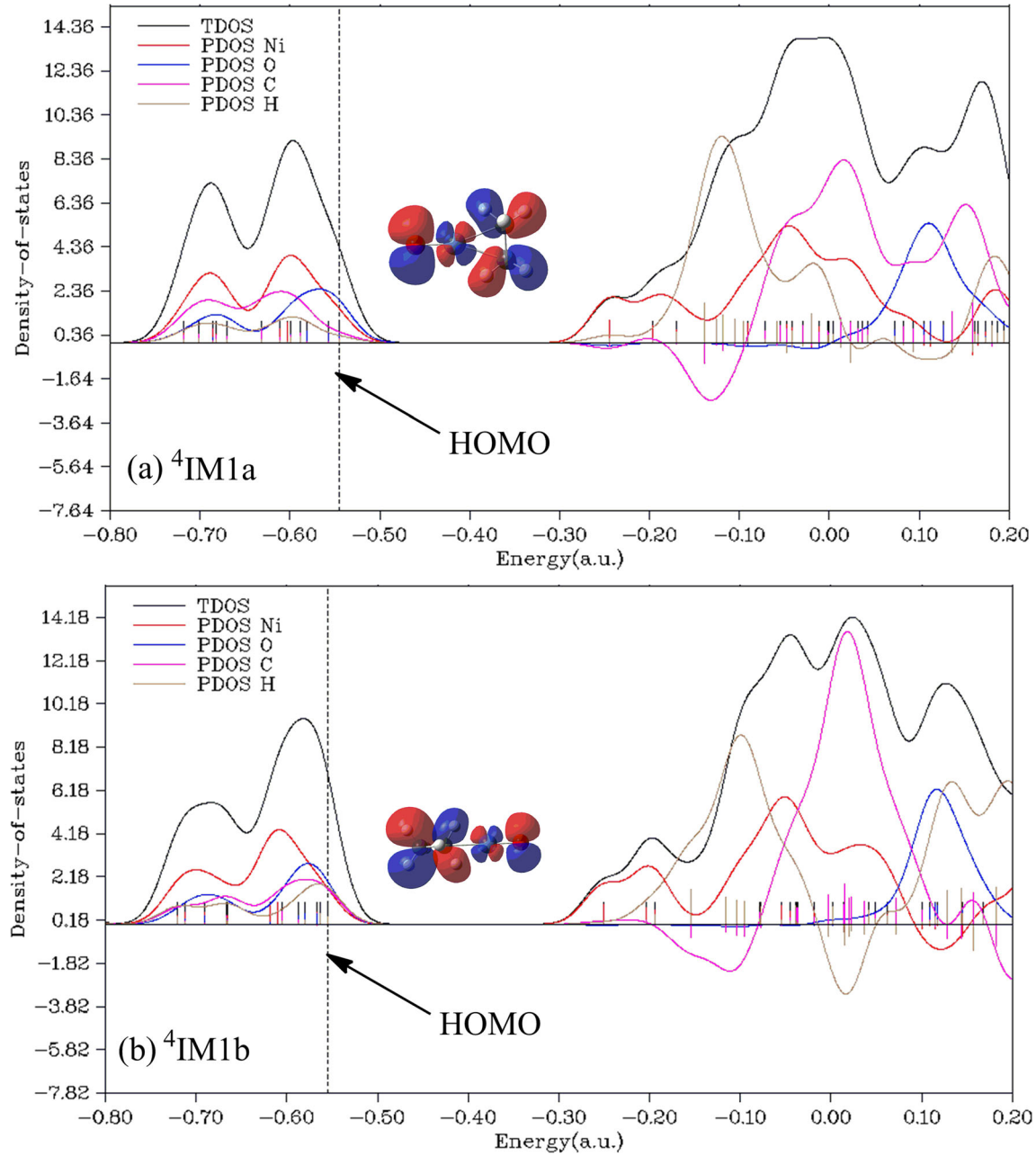

Fig. 4 The DOS curves for initial complexes. **a** Intermediate ^{4}IM1a. **b** Intermediate ^{4}IM1b

C_2H_6 and $^4NiO^+$ fragments, the horizontal lines in the middle represent for the complex orbital. It is clearly shown in Fig. 3 that both ^{4}IM1a and ^{4}IM1b have three single occupied molecular orbitals (SOMO), and the SOMO-1 of both initial complexes is the HOMO. The SOMO-1 of ^{4}IM1a(C_s), which has a a'' spatial symmetry, is composed by e_g orbital of C_2H_6 and $e_1(\pi)$ (Ni, d_{xz}; O, p_x) orbital of $^4NiO^+$. The lowest unoccupied molecular orbital (LUMO), which is composed by e_u orbital of C_2H_6 and $a_1(\sigma)$ (Ni, s; O, p_z) orbital of ^{4}NiO, has a a' spatial symmetry. While the LUMO of ^{4}IM1b(C_s), which is composed by a_{2g} orbital of C_2H_6 and a_1(Ni, s; O, p_z) orbital of $^4NiO^+$, has a a' spatial symmetry. The SOMO-1 of ^{4}IM1b(C_s), which has a a'' spatial symmetry, is composed by e_g orbital of C_2H_6 and $e_1(\pi)$ (Ni, d_{yz}; O, p_y) orbital of $^4NiO^+$. Moreover, the DOS analysis (see Fig. 4) shows that the PDOS-Ni curve and PDOS-O curve are high enough in a region of 1.36–2.36 (1.18–2.18) of ^{4}IM1a (^{4}IM1b), which means that the e_1 orbital of $^4NiO^+$ contributes a lot to the HOMO (SOMO-1) of ^{4}IM1a and ^{4}IM1b.

Curtin-Hammett principle analysis

The Curtin-Hammett principle (CHP) [39, 40] is an important concept in physical organic chemistry and is widely used in

finding the main product between the two product channels. It tells us that the product is not determined by the structure of the reactants, but rather by the relative height of the highest energy barrier of the different products, and the branching ratio of product depends only on the difference in barrier height between the two product channels.

Herein, we employ CHP to find out the proportion of products for the reaction of NiO^+ and C_2H_6. As shown in Fig. 5, the free energy of ^{2}TS2-1 is 25.06 kJ/mol higher than ^{2}TS2-2 ($\Delta\Delta G^{\neq} = 25.06$ kJ/mol), which indicates the competition product ratio of ^{2}IM2 → ^{2}IM3-1/^{2}IM3-2 amounts to approximately 4.06×10^{-5} (289.15 K). That is to say, ^{2}IM2 → ^{2}IM3-2 has an absolute advantage in the partitioning between two reaction channels, which is consistent with the experimental result [24, 25]. It is worth mentioning that the theoretical analysis that also suggests the ^{2}IM2 → ^{2}IM3-2, which has the lower reaction barrier, is the main reaction channel and the water and ethylene are the main products, which is in good agreement with the CHP analysis.

Bonding analysis

In order to gain a deeper understanding of the reaction mechanism, three different analysis methods (AIM, ELF, and NBO) are used in the title reaction pathways. Here, wavefunction files (.wfn) produced by Gaussian 09 were used as input files of Multinwfn to perform AIM and ELF analysis. The ELF plots of all transition states and intermediates along the reaction pathways are shown in Fig. 6. All the AIM parameters [41] of bcp are listed in Table S1. As we can see in Table S1, the AIM analyses include five aspects: $\rho(r)$, $\nabla^2\rho(r)$, $G(r)$, V(r), and $E(r)$. The $\rho(r)$ and $\nabla^2\rho(r)$ indicate the value of electron density and its Laplacian of electron density at (3, − 1) critical points, respectively. Besides, Lagrangian kinetic energy $G(r)$ stands for the speed of the electrons move; the potential energy density $V(r)$ stands for the degree of the electrons localized

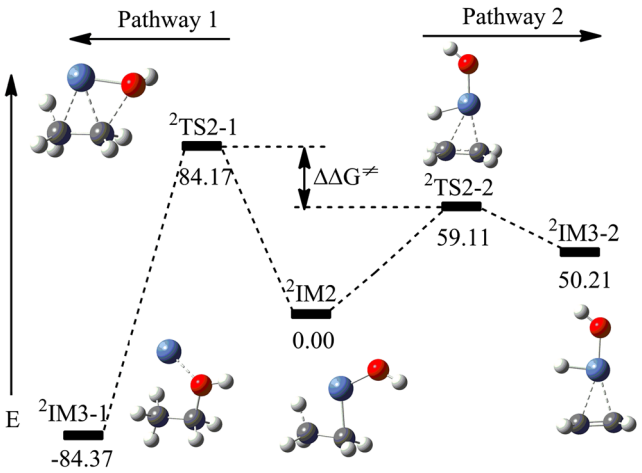

Fig. 5 Energy ($\Delta G^{\neq}$) diagrams of the reactions of ^{2}IM2 → ^{2}IM3-1 and ^{2}IM2 → ^{2}IM3-2 (the relative Gibbs energies in kJ/mol)

in the regions and $E(r)$ stands for the total electron energy density, $E(r) = G(r) + V(r)$. The value of $E(r)$ was proven to be an applicable method to character the nature of bonds for heavy-atom systems [37, 42]. A negative $E(r)$ and a positive $E(r)$ suggest covalent character and close-shell interaction, respectively [42].

(1) IM1a. The ELF analysis of IM1a tells us that there is an absence of disynaptic valence basin between the Ni and C1, C5 atoms, which indicates that the interaction is considered to be an electrostatic interaction. The AIM analysis also shows that a bcp (3, − 1) exists between Ni and C1, C5 atoms, but the corresponding density is very low ($^2\rho$(Ni-C1) = 0.052 au, $^2\rho$(Ni-C5) = 0.051 au, $^4\rho$(Ni-C1) = 0.047 au, $^4\rho$(Ni-C5) = 0.047 au). The $\nabla^2\rho(r)$ is small and positive (0.220 au for ^{2}Ni-C1 bond, 0.212 au for ^{2}Ni-C5 bond, 0.201 au for ^{4}Ni-C1 bond, 0.201 au for ^{4}Ni-C5 bond), indicating the loose charge density at the critical point; the energy density $|E(r)|$ is also small, although $E(r)$ is negative (− 0.003 au for ^{2}IM1-a, − 0.002 au for ^{4}IM1-a). All of the evidences above have proven that no bond is formed between Ni and C atoms of IM1a.

(2) IM1b. The NBO analysis shows that no bond is formed between Ni and C1 atoms. The ELF analysis also confirms this. It is clearly shown that there is an absence of disynaptic valence basin between Ni and C1 atom. According to the AIM analysis, a bcp (3, − 1) exists between the Ni and C1 atoms with the low corresponding density ($^2\rho$(Ni-C1) = 0.055 au, $^4\rho$(Ni-C1) = 0.057 au), and the low negative energy density ($E(r)$ = − 0.006 au for ^{2}IM1-b,$E(r)$ = − 0.007 au for ^{4}IM1-b), also indicating that no covalent bond is formed between Ni and C atoms of IM1-b.

(3) IM2. With the migration of H3, V(O-H3) basin is formed in this stage (from ELF analysis), which is consistent with the NBO analysis (BD(O-H3) = 0.868($sp^{3.13}$)O + 0.497(s)H3). ELF analysis also shows the existence of a weak disynaptic valence basin between the Ni and C1 atom, which is confirmed by the AIM analysis that the bcp (3, − 1) existing between Ni and C1 atom increases a lot. The corresponding density (ρ(Ni-C1)) increases to 0.116 au (0.162 au) on doublet (quartet) state; the $|E(r)|$ is relatively large, although $E(r)$ is still negative ($E(r)$ = − 0.037 au for ^{2}IM2, $E(r)$ = − 0.055 au for ^{4}IM2), indicating that the Ni-C1 bond of IM2 is comparatively stable. The fact is also proven by NBO analysis (BD(Ni-C1) = 0.814($sp^{0.16}d^{1.37}$)Ni + 0.581($sp^{14.47}$)C1).

(4) IM3-1. The linkage between Ni and C1 is completely broken in this phase. The AIM analysis shows that there is a bcp (3, −1) that exists between O and C1 atoms with a relatively large corresponding density ($^2\rho$(O-C1) = 0.225 au, $^4\rho$(O-C1) = 0.205 au); the $|E(r)|$, although is still negative, also increases a lot ($E(r)$ = − 0.284 au for

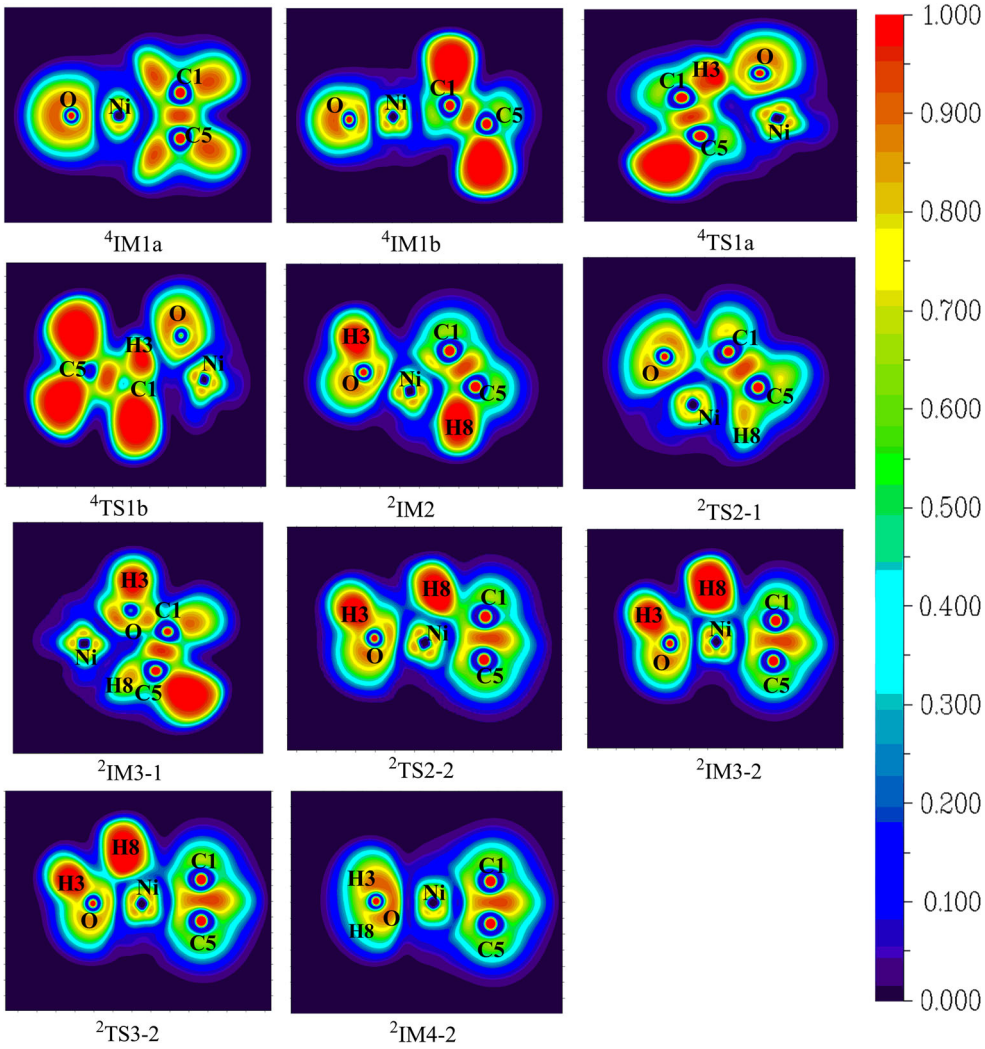

Fig. 6 ELF projection map of the lowest energy minima and transition states on the $NiO^+ + CH_3CH3$ reaction pathway at UB3LYP/6-311++G(3df,3pd) level of theory

doublet, $E(r) = -0.253$ au for quartet), which indicates the formation of O-C1 bond. And the ELF analysis also confirms this with a V(O-C1) basin formed.

(5) IM3-2. Compared with IM2, the linkage of C1 atom and H8 atom is getting smaller. The V(Ni-H8) basin is formed in this stage, which is consistent with the NBO analysis (BD(Ni-H8) = 0.710(s)Ni + $0.704(sp^{0.35}d^{0.91})$H8). The NBO analysis also shows that the C1-C5 bond has changed into a double bond, which is composed of σ bond and π bond (BD(C1-C5) = $0.710(sp^{1.65})$C1 + $0.704(sp^{1.65})$C5, BD(C1-C5) = $0.732(sp^{76.82})$C1 + $0.681(sp^{99.99})$C5).

(6) IM4-2. According to the ELF analysis, the V(O-H3) basin is replaced by the V(H8-O-H3) basin, indicating the formation of O-H8 bond. NBO analysis also confirms that. The formation of H_2O causing the disappear of Ni–O bond, which is evidenced by NBO analysis. The AIM analysis indicates that the binding of Ni^+ with H_2O and C_2H_4 units are both electrostatic interactions in ^{2}IM4-2, which is also confirmed by ELF. Conversely, the AIM analysis of ^{4}IM4-2 shows that the binding in $Ni(H_2O)^+$ unit performs as electrostatic interaction; whereas a relatively strong bcp (3, −1) exists between Ni atom and C5 atom in $Ni(C_2H_4)^+$ unit ($^2\rho$(Ni-C1) = 0.278 au, $E(r) = -0.289$ au) indicating the formation of Ni-C5 bond. This unbalanced binding situation among ^{4}IM4-2 ($\Delta E_R = -236.2$ kJ/mol) makes the complex weaker in stability than ^{4}IM4-2 ($\Delta E_R = -454.5$ kJ/mol).

Conclusions

The theoretical calculations have been performed to investigate the detailed mechanism of the gas-phase reaction of C_2H_6 with NiO^+ using density functional theory. All stationary points of doublet and quartet states in the reaction system are fully optimized using (U)B3LYP/6-311++G(3df,3pd) U SDD level of theory. The CHP is used to find out the

proportion of product for the reaction. From the calculations, the following conclusions emerged:

(1) We find that there are two processes for C_2H_6 oxidation by NiO^+, which differs based on the linkage of NiO^+ with ethane via Ni^+, but both processes can form $(C_2H_5)Ni^+(OH)$ through a C-H activation. Starting from $(C_2H_5)Ni^+(OH)$ (IM2), the system can take place along two reaction pathways, one is the coupling of Ni^+ and O atom to form Ni^+ and C_2H_5OH, the other is the stepwise β-H immigration to form $Ni(C_2H_4)^+ + H_2O$ and $Ni(H_2O)^+ + C_2H_4$.

(2) The Curtin-Hammett principle calculation results suggest that the ratio of ethanol, water, and ethylene is 4.06×10^{-5}, indicating that pathway 2 is the main reaction channel and the water and ethylene are the main products.

(3) The AIM and ELF analyses suggest that the interaction between NiO^+ and C_2H_6 is considered to be an electrostatic interaction in the complex IM1a and IM1b. Additionally, the DOS analysis also shows that the $e_1(\pi)$ orbital of $^4NiO^+$ contributes a lot to the HOMO of ^{4}IM1a and ^{4}IM1b.

Funding information We are grateful to the financial support from the National Natural Science Foundation of China (Grant No. 21263023) and support from the Supercomputing Center of Gansu Province.

Compliance with ethical standards

Conflict of interest The authors declare that they have no competing interests.

References

1. Li LC, Liu JL, Shang J, Wang X, Wong NB (2008). J Theor Comput Chem 6:323–330
2. Deryan Hwang AMM (2007). J Phys Chem A 106:12072–12083
3. Li FM, Yang HQ, Ju TY (2012). Comput Theor Chem 994:112–120
4. Balcells D, Clot E, Eisenstein O (2010). Chem Rev 110:749–823
5. Greene TM, Andrews L, Downs AJJ (1995). Am Chem Soc 117: 8180–8187
6. Kafafi ZH, Hauge RH, Margrave JL (1985). J Am Chem Soc 107: 6134–6135
7. Andrews L, Cho H-G (2006). Organometallics 25:4040–4053
8. Wittborn AMC, Costas M, Blomberg MRA (1997). J Chem Phys 107:4318–4328
9. Holthausen MC, Fiedler A, Helmut SA (1996). J Phys Chem 100: 409–429
10. Zhang DJ, Liu CB, Liu YJ (2010). Chinese J Chem 20:220–226
11. Sahoo S, Reber AC, Khanna SN (2015). J Phys Chem A 119:12855
12. Eller K, Schwarz H (1991). Chem Rev 91:1121–1177
13. Roithvá J, Schröder D (2010). J Phys Chem A 110:1170–1211
14. And YS, Yoshizawa K (2000). J Am Chem Soc 122:12317–12326
15. Yoshizawa K, Shiota Y, Yamabe T (2010). Chem Eur J 3:1160–1169
16. Schröder DCD, Angew SH (1990). Chem Int Edit 29:1431–1433
17. Sun XL, Huang XR, Li JL, Huo RP, Sun CC (2012). J Phys Chem A 116:1475–1485
18. Schröder D, Schwarz H, Clemmer DE (1997). Int J Mass Spectrom 161:175–191
19. Jackson TC, Jacobson DB, Freiser BSJ (1984). Am Chem Soc 106: 1252–1257
20. Schröder D, Angew SH (1990). Chem Int Ed Engl 29:1433–−1434
21. Schröder D, Fiedler A, Hrusak J, Schwarz H (1992). J Am Chem Soc 114:1215–1222
22. Ryan MF, Fiedler A, Schröder D, Schwarz H (1994). Organometallics 13:4072–4081
23. Zhao L, Lu X, Li Y, Chen J, Guo WJ (2012). Phys Chem A 116: 3282–−3289
24. Schuurman Y, Ducarme V, Chen T, Li W, Mirodatos C, Martin GA (1997). Appl Catal A 163:227–235
25. Chen T, Zi LW, Yu CY (1999). Acta Chim Sin 57:986–991
26. Skoufa Z, Heracleous E, Lemonidou AA (2015). J Catal 322:118–129
27. Zhu H, Dong H, Laveille P (2014). Catal Today 228:58–64
28. Solsona B, Concepción P, Hernández S (2012). Catal Today 180: 51–58
29. Frisch MJ, Trucks GW, Schlegel HB, Scuseria GE, Robb MA, Cheeseman JR,Scalmani G, Barone V, Mennucci B, Petersson GA, Nakatsuji H, Caricato M, Li X, Hratchian HP, Izmaylov AF, Bloino J, Zheng G, Sonnenberg JL, Hada M, Ehara M, Toyota K, Fukuda R, Hasegawa J, Ishida M, Nakajima T, Honda Y, Kitao O, Nakai H, Vreven T, Montgomery JA. Jr., Peralta JE, Ogliaro F, Bearpark M, Heyd JJ, Brothers E, Kudin KN, Staroverov VN, Kobayashi R, Normand J, Raghavachari K, Rendell A, Burant JC, Iyengar SS, Tomasi J, Cossi M, Rega N, Millam JM, Klene M, Knox JE, Cross JB, Bakken V, Adamo C, Jaramillo J, Gomperts R, Stratmann RE, Yazyev O, Austin AJ, Cammi R, Pomelli C, Ochterski JW, Martin RL, Morokuma K, Zakrzewski VG, Voth GA, Salvador P, Dannenberg JJ, Dapprich S, Daniels AD, Farkas Ö, Foresman JB, Ortiz JV, Cioslowski J, Fox DJ (2009) Gaussian 09, Revision D.01, Gaussian Inc., Wallingford, CT
30. Lee C, Yang W, Parr RG (1988). Phys Rev B: Condens Matter Mater Phys 37:785
31. Beck JE, Dudley TJ (2017). J Phys Chem A 121:1715
32. Gonzalez C, Schlegel HB (1989). J Chem Phys 90:2154
33. Carlos Gonzalez, H. Bernhard Schlege. (1990) J Phys Chem 94: 5523–5527
34. Lu T, Chen F (2012). J Comput Chem 33:580
35. Becke AD, Edgecombe KE (1990). J Chem Phys 92:5397–5403
36. Wang XL, Wang YC, Li S, Zhang YW, Ma PP (2016). J Phys Chem A 120:5457–5463
37. Bader R (1990) A quantum theory. Clarendon, Oxford
38. Zhao LM, Guo WY, Liu ZC, Li YY, Lu XQ (2011). Theor Chem Accounts 128:349–358
39. Haupert LJ, Poutsma JC, Wenthold PG (2010). Cheminform 41: 1480–1488
40. Jin YZ, Wang YC, Ji DF (2013). Comput Theor Chem 1011:75–81
41. Cremer D, Kraka E (1984). Angew Chem Int Ed Engl 23:627–628
42. De Almeida K, Ramalho T, Neto J, Santiago R, Felicíssimo V, Duarte H (2013). Organometallics 32:989–999